INFLUENCE OF COMPONENT DESIGN ON FEATURES AND PROPERTIES IN THERMOPLASTIC OVERMOULDED COMPOSITES

M. A. Valverde[1,2*], R. Kupfer[2], T. Wollmann[2], L. Kawashita[1], M. Gude[2], S. R. Hallett[1]

[1] Bristol Composites Institute (ACCIS), University of Bristol, Bristol, BS8 1TR, UK
[2] Institute of Lightweight Engineering and Polymer Technology (ILK), Technische Universität Dresden, 01037 Dresden, Holbeinstr. 3, Germany.
*Corresponding author (mario.valverde@bristol.ac.uk)

Abstract
Thermoplastic composite overmoulding is an integrated process to manufacture components with combined continuous and short fibre reinforcements. These components benefit from high intrinsic mechanical properties, geometric complexity and low production cycle times. In this study, ribbed plates were manufactured by overmoulding short-fibre CF/PPS (carbon fibre/polyphenylene sulphide) material onto continuous woven-fibre CF/PPS flat preforms. Specifically, the effects of the rib geometry and flow length on the process-induced features were investigated using optical microscopy. The bonding at the overmoulded interface was evaluated via quasi-static tensile rib pull-off tests. Results indicate that both the bond strength and corresponding failure type vary with rib geometry. However, the effects of the specimen position along the flow length are only significant towards the end path. The implications of certain rib designs are discussed both qualitatively and quantitatively, based on feature development at the overmoulded interface during manufacture.

Keywords: (A) *Thermoplastic matrix; (B) Physical properties; (D) Mechanical testing; (E) Overmoulding.*

1. Introduction

Thermoplastic composites have gained considerable attention over the past decades as they exhibit certain advantages over thermosets; increased fracture toughness, chemical resistance and potential for recyclability to name a few, making them well suited for the next generation of high-performance composite structures [1]. From a manufacturing perspective, the increasing demand for aerospace components has encouraged the idea of thermoplastics replacing existing metals and thermosets due to their potential for out-of-autoclave (OOA) processing, automation and rapid joining capabilities, where the costs are offset by the high-volume production [2]. Though thermoplastic composites have seen commercial and military use, such as the A340-600 J-nose and A400M cockpit floor panels [3], their applications are limited to rather simple geometries, given that continuous fibre preforms are challenging to shape and excessive forming of the material can result in fibre buckling and wrinkling [4, 5]. In contrast, high-volume manufacturing sectors such as the automotive industry can produce relatively complex parts using injection moulded short fibre reinforced material, although the intricate features and low cycle time benefits come at the expense of material's mechanical performance [6]. Such a design trade-off can be addressed by thermoplastic composite overmoulding, an integrated manufacturing process, combining thermoforming and injection moulding technologies, that has enabled the rapid manufacture of composite structures with both continuous and short fibre reinforcements [7-9]. These components benefit from the excellent mechanical properties provided by the continuous fibre preform, geometric complexity of the short fibre-reinforced injection moulded architecture and significantly reduced cycle times due to the fast processing of thermoplastics [10, 11]. This multi-material design is particularly well suited for high-volume manufacturing applications where structural performance is critical and would otherwise be difficult to achieve with traditional thermoplastic processing techniques alone. The injection moulded substructure, typically serving as stiffening, impact absorbing or functional features, can be tailored to carry significant loads. It is hence important to ensure a strong bond at the overmoulded interface, between the continuous and short fibre material. The use of thermoplastic overmoulded composites has grown in the past decade within the

automotive industry, where examples include the brake pedal for the 918 Porsche Spyder, demonstrated for volume production as part of a pre-development project by *ZF Friedrichshafen* [12]. In addition, the manufacturing approach employed by *Herone GmbH* for carbon fibre-thermoplastic geared driveshafts (Figure 1), although still in development, demonstrates the ability to exploit overmoulding for a wide range of structural aerospace applications [13].

Figure 1: Prototype continuous CF-PAEK driveshaft overmoulded with a short CF-PEEK gear, supplied by *Victrex Europa GmbH* [14].

Given that overmoulding is both an integrated forming and joining technology, one of the key challenges is the prediction of the degree of bonding at the overmoulded interface, where the preform and injected compound material interact under high temperature and pressure conditions in a short time period [15]. Such joints tend to be the weakest points of a structure, leading to significant weight penalties if not designed properly [16]. Fusion bonding has long been used to describe the processing of thermoplastic and thermoplastic composite materials. For semi-crystalline polymers, such as PPS, the required processing temperatures are usually at least 40 °C above the melting point (T_m=280 °C) [17]. Under these conditions the material is able to flow, due to the reduced viscosity, and form close contact between the two adhering surfaces - a phenomenon referred to as intimate contact. Only in the areas where intimate contact is achieved can healing (interdiffusion of polymer chains across the material interface) occur. The degree of healing, described by equation (1), is a temperature- and time-dependent process and is described by the reptation theory of linear polymer chains [15]. The fracture stress of the bonded interface is proportional to the fourth root of time, t, spent under processing conditions, t_R is the reptation time (a function of temperature) and σ_∞ is the strength of the neat polymer [17].

$$D_h(t) = \sigma = \sigma_\infty \left(\frac{t}{t_R}\right)^{\frac{1}{4}} \qquad (1)$$

Common methods to evaluate the bonding between two thermoplastics include: 1) tensile loading in the direction normal to the preform surface, 2) shear loading in the plane of the preform surface, and 3) peeling such that progressive separation of the adhering surfaces is achieved. These studies tend to involve characterisation of the resistance to mode I crack propagation along a bonded interface with a linear elastic fracture mechanics-based test. The results are then expressed as a variation of the critical stress intensity factor, K_c, or the critical strain energy release rate, G_c, with the bonding time and temperature [18]. These theories have been widely used to describe the bonding of amorphous thermoplastics under isothermal processing conditions [19], which is not the case in overmoulding processes. This is because the injected material has a very short time to fuse to the preform before both materials solidify, given the rapid heat loss to the colder mould tool, making quantification of the bond strength a challenging task. The presence of fibres may also affect the bonding.
Giusti et al. [20] conducted tensile tests on custom-designed overmoulded specimens, based on ISO 527, to investigate the bond strength between twill weave GF-PA6 flat organosheet preforms and half-dumbbell GF-PA66 injected compounds manufactured at different process settings. Higher injection temperatures and injection speeds were seen to improve the bond strength, suggesting that the flow behaviour of the compound material, which can be easily controlled via the injection machine settings, is a key factor influencing the mechanical performance of the overmoulded interface. Whilst the

inherent design of “as-moulded” coupons are suitable for evaluating the bonding characteristics for pre-defined welding locations in detail, limited information can be obtained about the bonding of an as-manufactured component. This is due to the flow behaviour of the injected material for different flow path lengths and cross-sectional areas, as it effectively changes the morphology of the material. This in turn can affect the fibre orientation, which has a major influence on the mechanical properties of the final component, as the fibres will tend to align in the direction of the flow through the injection cavity. In these directions, the material is also expected to shrink more due to the mismatch in coefficient of thermal expansion (CTE.) The rapid and non-isothermal nature of the overmoulding process means that control of the fibre orientation is thus difficult, as it is fundamentally determined by the component design (mould geometry), material system and process settings [21]. In order to investigate the key process-property relations, test specimens ought to be extracted from the as-manufactured component in order to capture the consolidation characteristics and geometry-dependent features specific to each processing condition, given that the effects of tool geometry and process settings on fibre orientation and void content have been reported for injection moulded and overmoulded parts [22-24, 35]. Joppich et al. [25] assessed the overmoulded interface behaviour of three CF-PEI/GF-PEI specimens, designed for tensile, shear and peel stress respectively. The behaviour of the overmoulded coupons were seen to have a large variance in tensile strength (28.2 %), however this value was lower when samples were compared from the same positions throughout the parts. Few studies have considered the process-induced features at the overmoulded interface, such as the local out-of-plane deformations reported by Stegelmann et al. [26] and Valverde et al. [27], where the interaction with the clamping tool cavity locally affects the compaction of the continuous fibres. Hence, investigating how the overmoulded interface develops during the manufacturing process and is affected by the component design allows for an understanding of the consolidation characteristics at the overmoulded interface and subsequent properties. This is vital, given the strict certification requirements imposed by the aerospace industry.

It is important to mention that there are no standard methods for assessing the degree of bonding in overmoulded components [28] as it is dependent on many factors that are very difficult to control: process parameters, mould design and material system – all of which can in turn influence crystallinity, fibre orientation, residual stresses, void content, geometry of the overmoulded interface. Due to the nature of the manufacturing process, a change in one variable can affect several others. For example, if a consistent level of preform deformation (induced during the closing of the mould tools) is required across a range of injection moulded substructure geometries, the process settings, such as the clamp force or holding (sometimes referred to as packing) pressure profile, must be varied. Yet, in doing so, the properties of both the injected material and preform will be affected, as has been previously reported [29]. This process-property dependence is common in plastics processing and has historically been tackled through rigorous experimental programmes, which have proven costly and time-consuming. Hence, an investigation into a select number of factors that affect the features and properties in overmoulded components should be addressed in current and future overmoulding studies.

In this study, thermoplastic composite ribbed plates of varying rib geometry were manufactured by overmoulding short-fibre material onto continuous woven-fibre preforms using a standard injection moulding machine. This allowed for an investigation into the effects of the mould geometry (rib feet) for one material combination and choice of process settings, so to prevent additional factors from influencing the studied features. The quality was investigated via mechanical testing of the rib-base plate joint as well as optical microscopy to quantify the following process-induced features: fibre orientation, void content and preform deformation, given that the overmoulded interface is the load-carrying area between the two substructures.

Materials and Design

The overmoulded ribbed plate (Figure 2) consists of a 2.52 mm thick base plate with four injection moulded ribs of different feet width and height, as can be seen in Figure 3. This component is typical of an aerospace structure, where a composite panel is reinforced with additional elements for local stiffening. Commercially available 5-Harness Satin (5HS) *Cetex® TC1100* CF/PPS organosheets, supplied by *TenCate Advanced Composites,* were autoclave consolidated at 320 °C in a $[0/90]_4$ layup

sequence for one hour, cut into the required dimensions and cleaned with acetone prior to overmoulding. The compound material used was a 33 % high modulus short-carbon fibre reinforced PPS compound (*Luvocom® 1301-0824*), supplied in 3 mm-long pellets by *Lehmann & Voss*. This type of compound material was used due to its relatively high mechanical properties compared to the neat matrix equivalent. By using a fibre-filled compound, the mismatch between the thermal expansion coefficients (CTEs) of the two substructures is minimised. The matrices for the two substructure materials are both linear and semi-crystalline.

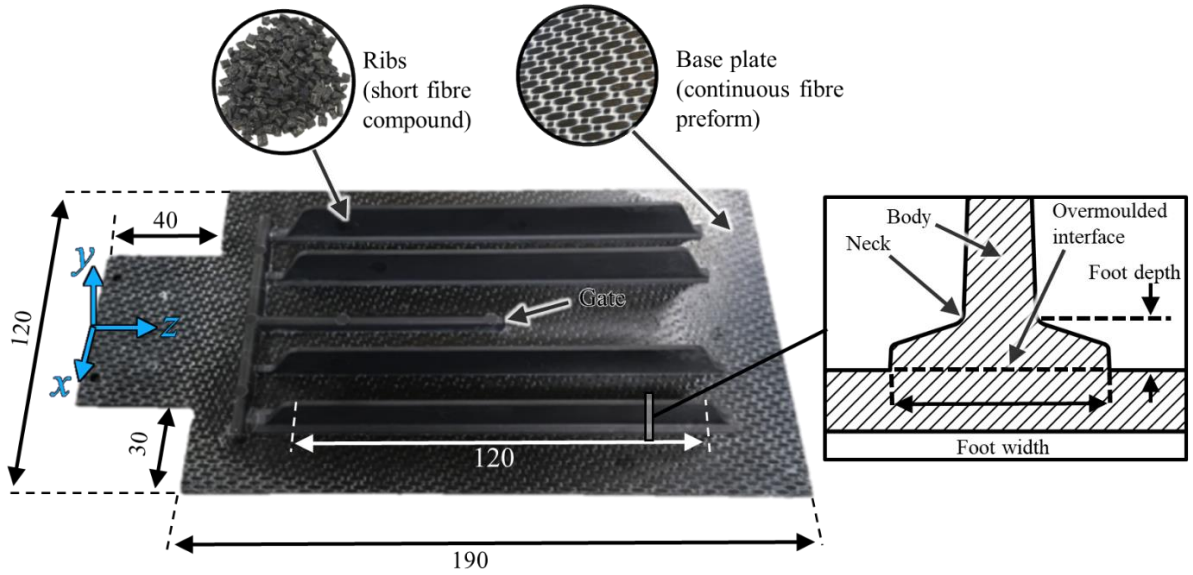

Figure 2: Overmoulded ribbed plate component, showing multi-material construction and variation in rib foot design. All dimensions shown are in mm.

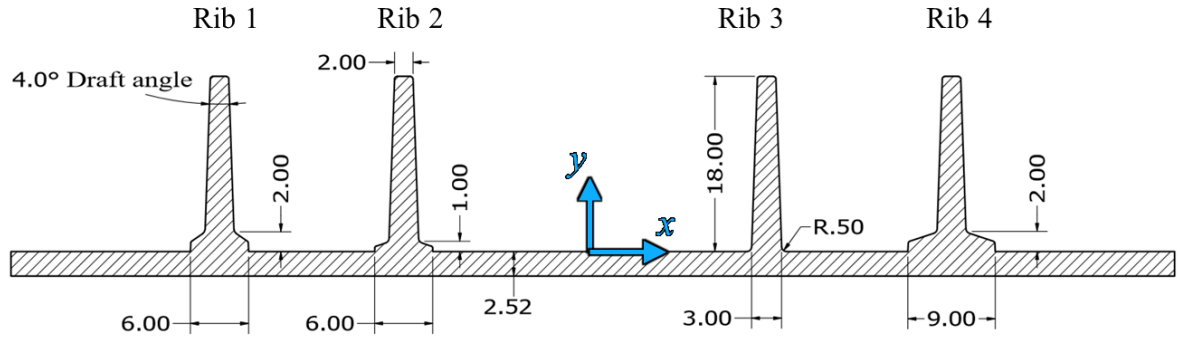

Figure 3: Ribbed plate cross-section, showing key dimensions (in mm) for all four rib designs.

Manufacturing Description

The manufacturing process is divided into seven stages, where both the preform and compound materials are melted, formed and cooled under highly dynamic temperature/pressure profiles, resulting in fusion bonding and subsequent fabrication of the overmoulded component, as can be seen in Figure 5. An injection moulding machine (ARBURG ALLROUNDER 270 C 500-200) was adapted with an in-mould heating station and used for this study. Two guide pins were mounted on the injection tool and used to manually fix the position of the preform prior to the start of each cycle. The compound material was dried for 4.0 hours at the glass transition temperature (90 °C) prior to processing, as recommended by the datasheet, although CF/PPS has been shown to have very low water absorption [30]. Finally, a hole was drilled in the centre of the preform so that the compound material is able to enter the mould cavity. The choice of process settings was based on preliminary work conducted at the

TU Dresden on CF/PPS overmoulded composites and Autodesk MoldFlow© simulations. The results of the MoldFlow studies generated a range of process settings for which an acceptable quality component would be moulded using the studied material, within the constraints of the ribbed plate geometry. Five ribbed plates were manufactured for this study and used for the characterisation of the fibre orientation, voids, preform deformations and overmoulded bond strength.

An infrared heater (KRELUS G14-25-2.5 MINI 7.5) was used to heat the preform, with a target temperature of 350 °C (recorded by an embedded pyrometer directed at the preform.) The emissivity used for the CF/PPS material is 0.90, as recommended in [31]. The temperature is further monitored by a K-type thermocouple fixed to the surface of the preform (as shown in Figure 4) during preliminary heating trials. Figure 4 shows that although the temperature at the surface did not reach 350 °C, it was above the matrix melting temperature of 280 °C for the duration of the transfer stage (defined as the time taken between the end of heating and start of the injection.) For these preliminary trials, the thermocouple remained fixed to the surface of the preform, without closing the mould halves, as otherwise the clamping force would damage the thermocouple and tool surface. During the 60.0 s heating stage, the surface temperature of the preform increased steadily by 10 °C. Upon completion of the pre-heating stage (Figure 5a), the heater (mounted on a vertical pneumatic arm) moved out of the way (Figure 5b) for the clamping tool to close, form and consolidate the continuous fibre preform, as the heating stage can induce deconsolidation. The temperature at the point of the mould closing onto the warm preform was 295 °C, as measured by the thermocouple during the preliminary heating experiments, indicating that a 15 °C drop in the surface temperature occurred for this particular overmoulding setup.

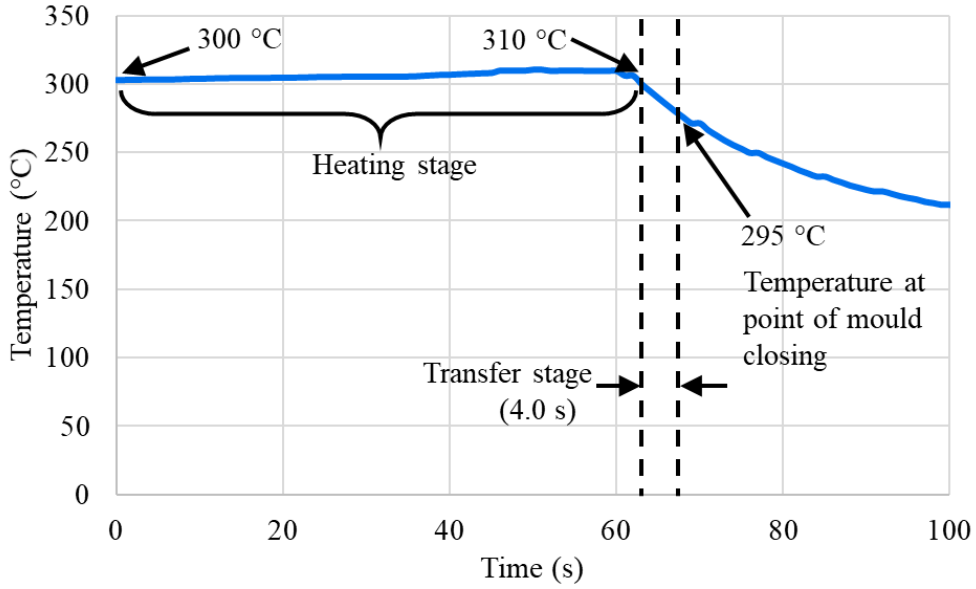

Figure 4: K-type thermocouple data during preliminary heating trials

The mould temperature was maintained at 145 °C using a hot oil control unit for the duration of the cycle. The clamping tool then closed and formed the preform with a 400 kN clamp force (Figure 5c), to ensure adequate consolidation and to prevent separation of the mould tools during the filling and holding stages, since the short fibre compound material imparts a high injection pressure on the clamping tool, as predicted by the preliminary MoldFlow simulations conducted on the ribbed plate component. During the filling stage (Figure 5d), the compound material was injected into the mould cavity at 325 °C and a 12 cm^3/s flow rate, where it filled the cavity and simultaneously bonded to the preform, given that semi-crystalline thermoplastics can be welded [32] above the T_m under pressure, as recommended by the material datasheet for TC1100 [33]. The exact temperature and pressure values can differ due to the different manufacturing techniques available, but for the case considered in this study, the values were derived from a typical thermoforming process, where the recommended processing temperatures and pressures are approx. 320 °C and between 10 – 40 bar respectively. After the compound material was injected, the holding pressure profile (650 bar for 6.0 s, 550 bar for 3.5 s

and 400 bar for 2.0 s) was applied to compensate for material shrinkage during cooling (Figure 5e) as well as to provide consolidation pressure at the overmoulded interface, thus eliminating void formation.

After the 30 s cooling stage, the compound material reaches the mould temperature (Figure 5f), the part was demoulded (Figure 5g), and the sprue cut off prior to further cooling to room temperature. The cycle time from the point at which the target temperature is reached to demoulding was approximately 140 seconds.

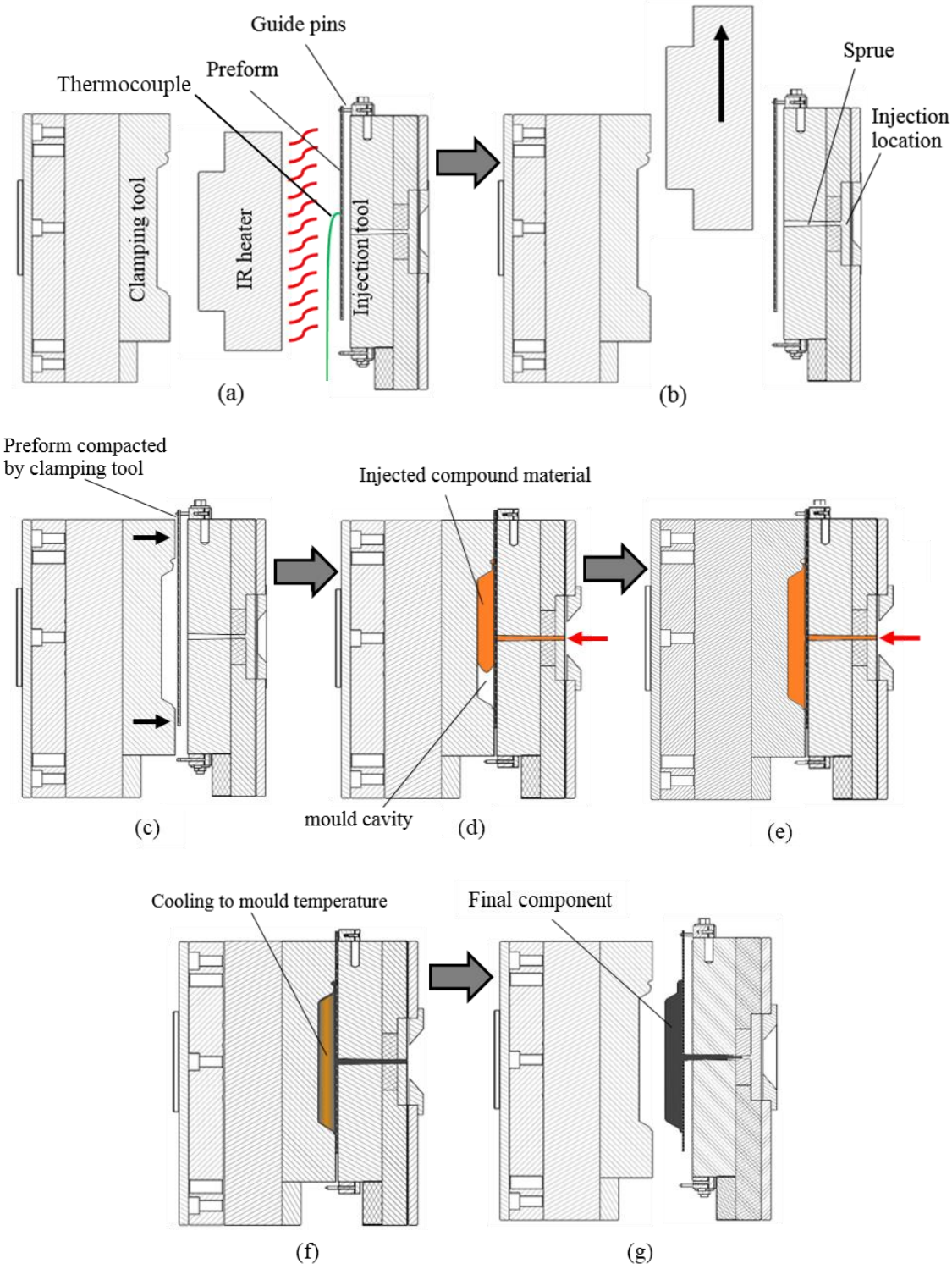

Figure 5: Section views of injection machine mould, showing (a) preheating, (b) transfer, (c) forming, (d) filling, (e) holding, (f) cooling and (g) demoulding stages.

Characterisation Methodology

A diamond-coated water-cooled saw was used to cut out specimens (one from each of the five manufactured ribbed plates) from the middle location of the flow length, thus ensuring similar flow-wise conditions across the four rib-plate interfaces, as seen in Figure 6. Specimens were further cut from the start and end of Rib 3 in order to compare the process-induced features and degree of bonding at different locations along the flow length, given that the injected compound material takes 2.70 s to fill the cavity. This is an inherent aspect of injection mouldings (and thus overmoulded components), and results in a temperature profile variation throughout the component, as the preform material loses more heat towards the end due to a prolonged exposure to the colder mould cavity. The preliminary MoldFlow simulations predicted a temperature drop of 15 °C in the centre of the preform in Rib 3 at the end location of the rib length compared to the start, although no experimental data was able to verify this due to the difficulties associated with in-situ temperature measurements for preform materials during overmoulding cycles. The pressure level is also associated with the location of the compound material in the cavity and is expected to be highest near the gate whilst at a minimum at the end of the flow path, further causing variations in the consolidation profile between the injected compound and preform material [34].

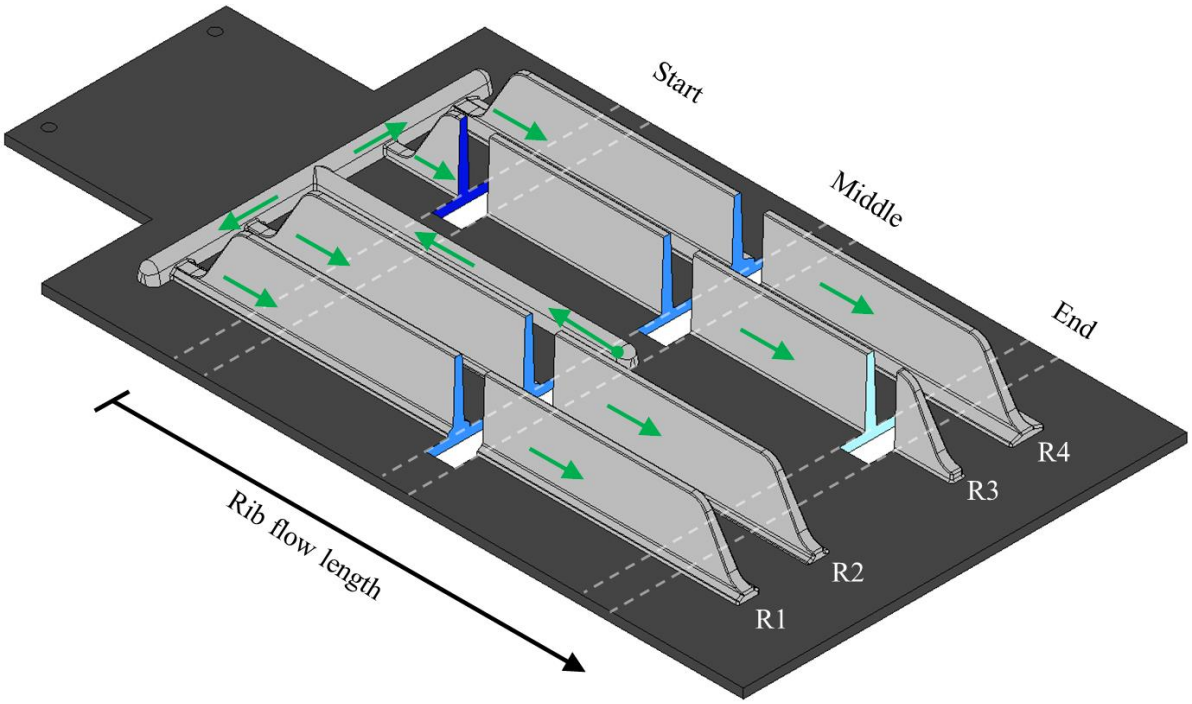

Figure 6: CAD model of ribbed plate component showing direction of injected compound material (green arrows) and specimen cut locations, where the start, middle and end are indicated by dark, normal and light blue colours respectively.

Micrograph Analysis

The microscopy specimens, Figure 6, were mounted in a fast-curing VersoCit-2 acrylic resin, ground, polished and analysed using a Carl Zeiss Imager M2 Optical Microscope at 20x magnification. The rib foot was chosen as the area to investigate for the fibre orientation analysis, given that the flow dynamics of the compound material are affected by the cavity geometry. On the micrographs, an elliptical footprint is produced for each fibre intersecting the xy-plane, where its orientation can be described by the angles (θ, ϕ) as shown in Figure 7. Seven sub-sections along the width of each micrograph (430 µm x 500 µm in size and located 1.5 mm above the rib base), see figure 8b, were processed using an automatic ellipse-fitting algorithm in the ImageJ software, where the semi minor and semi major axes for each intersecting fibre (superimposed by an ellipse) were computed. The use

of seven subsections allows for a simple visualisation of the fibre orientation changes throughout the rib widths. Equation (1) gives the angle of the fibre normal to the sectioned surface and thus can be used with equation (2) to calculate the individual orientation components in the flow direction (P_Z), using a technique based upon a method described by Bernasconi et al. and Advani et al. [24, 35]. These were averaged for each sub-section and used as an indication of the local fibre orientation.

$$\theta = cos^{-1}\left(\frac{b}{a}\right) \quad (1)$$

$$P_Z = cos(\theta) \quad (2)$$

The void content was calculated using an image thresholding technique based on the methods proposed by Santulli et al. [36] where the minimum measurement size was set to 38µm (based on an assumed 7µm carbon fibre diameter) to prevent the detection of scratches or cracked fibres. The preform deformation was taken as the measured distance between the nominal fibre path and the central midpoint of the uppermost deformed fibre in the layup. The size of the core region is approximated by manually fitting a curve to the region bounding the highly aligned fibres to the randomly oriented fibres as shown by the white dashed ellipse in Figure 8b and calculating the encompassed area.

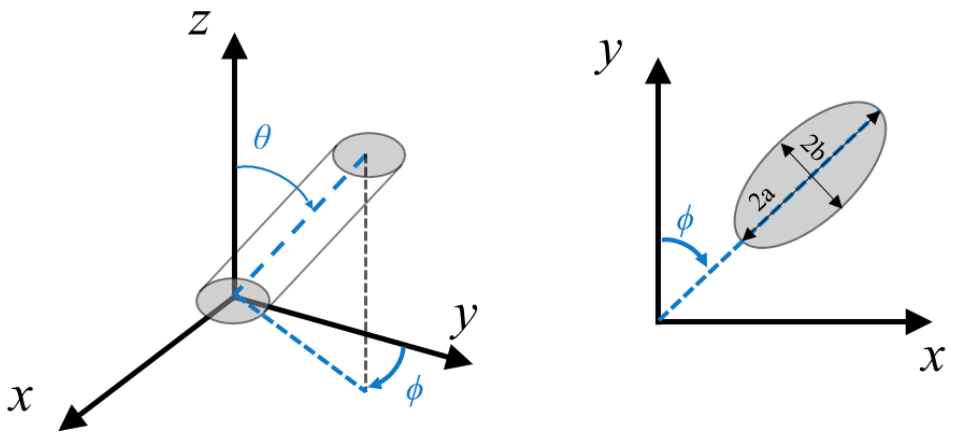

Figure 7: Coordinate system and definitions of angles θ and ϕ for a single fibre.

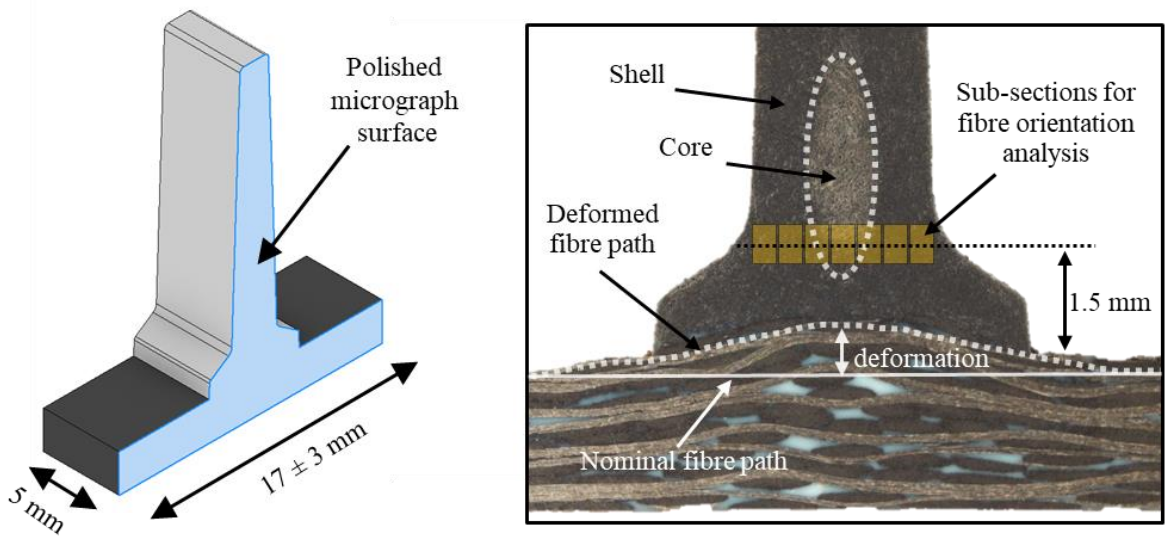

Figure 8: Microscopy specimen of Rib 1 (a) and micrograph highlighting key areas for characterisation techniques (b).

Mechanical Test Setup

A custom steel fixture was designed and manufactured for the testing of the mechanical specimens, ensuring that the base plate remains constrained when the ribs are pulled in tension. Replaceable clamping fixtures were used to ensure a sliding fit for the different rib widths. This isolated the overmoulded interface, that is expected to resist the applied load (Figure 9.) To account for the draft angle, the grips were rotated such that there was a uniform stress acting on both sides of the rib. The samples were sprayed with a light coat of white paint to aid in the analysis of the fracture behaviour and tested in a universal testing machine (Zwick 1445) at a 2 mm/min loading rate. The failure stress was taken as the peak load divided by the fracture area.

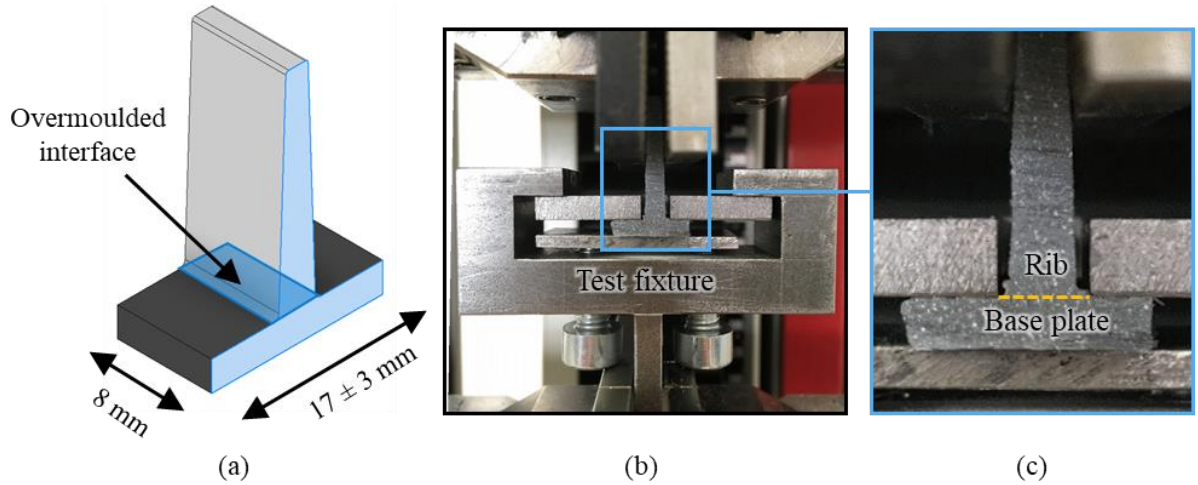

Figure 9: Mechanical specimen of Rib 3 (a) and setup of rib pull-off test (b), using custom built fixture for isolating the overmoulded interface (c).

Results and Discussion

Fibre Orientation

Analysis of the micrographs reveals a high level of orientation, suggesting that the fibres are generally aligned with the flow of the compound material. The width-wise distribution in fibre orientation is seen to vary between the four overmoulded ribs, clearly highlighting a drop at the centre, as seen in Figure 10. This pattern is common in injection moulded parts as the combination of shear and extensional flow during the injection of the compound material gives rise to the characteristic layered shell-core structure [37]. Just inward of the mould walls, where the material experiences the highest shear rates, the shell region is formed, as the fibres can align locally, thus resulting in high levels of orientation. The core region has the lowest shear rate as it remains hottest for longer, allowing the material to relax and results in low levels of orientation. When comparing the average flow-wise orientations of Rib 1 (0.72 ± 0.10) and Rib 2 (0.73 ± 0.11), a two-sample T-test presented no significant variation when tested for equal means at 95 % confidence. However, a clear difference is present between Rib 4 (0.63 ± 0.05) and Rib 3 (0.78 ± 0.12), showing the lowest and highest average fibre orientations respectively. This observation is expected as the ribs with smaller cross sections (Rib 3) can dissipate heat to the mould walls faster than ribs with larger cross sections, such as Rib 4. This is particularly important when designing overmoulded components, as opposed to conventional injection moulded parts, given that the residual heat from the preform alters the local temperature profile. This can result in a reduction in the fibre orientation in the flow direction, as the locally warmer material will have more time to relax, hence the orientation of the individual fibres will not be “frozen-in” as would be expected at regions near the colder mould walls.

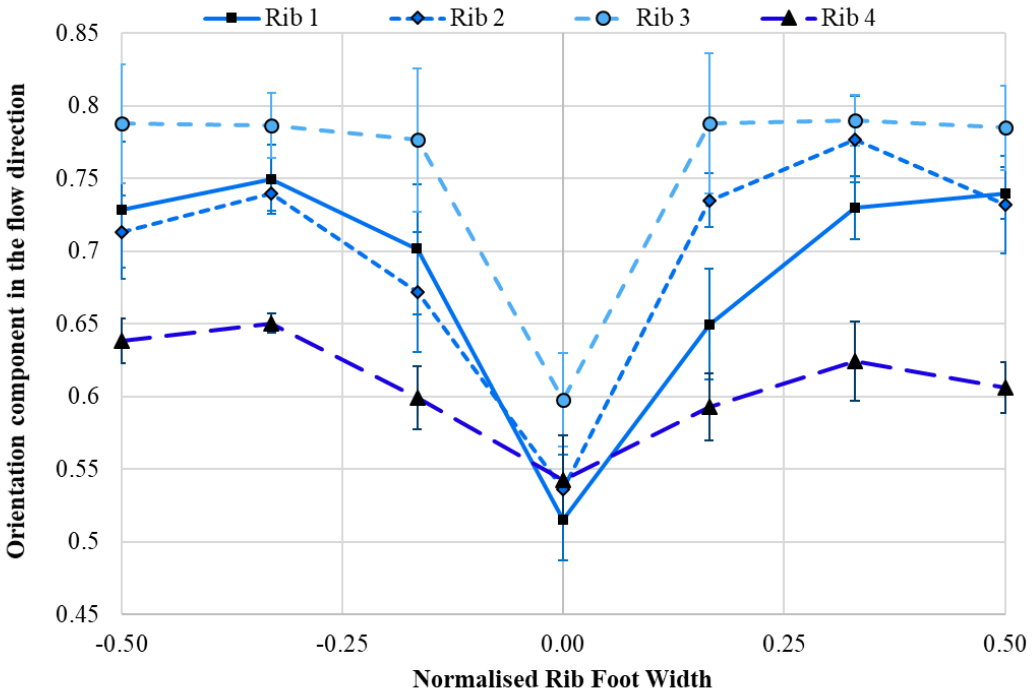

Figure 10: Fibre orientation components in the flow direction for each subsection along the rib width. Error bars indicate the standard deviation.

When comparing the micrographs taken from the different locations along the flow length of Rib 3, the average fibre orientation drops from 0.71 ± 0.08 at the start to 0.59 ± 0.10 at the end, with a slight peak at the middle (0.78 ± 0.12). The higher orientation components in the flow direction seen at the start and middle of the flow path are expected since the material is continuously flowing, bringing along new layers which shear past previous ones, allowing the shell region to develop until the material stops flowing. The micrographs further suggest that the shear flow is less prevalent at the end of the flow path, as can be seen by the large core area at the end of the flow path of Rib 3 [38]. Such effects are consequences of the highly complex material behaviour through the mould cavity (fountain flow), as the flowing compound material at a given point is solidifying and thus the newly formed solid layers are reducing the cross-section for the material to flow through. This will not be the case at regions further away from the gate, where the material is yet to arrive, potentially leading to differences in the shell-core structure. This implies that components with long injection lengths could suffer from warpage if the variation in the shell-core distribution along the flow length is significant. This is because the highly aligned shell will shrink more in the directions orthogonal to the flow, compared to the core region as it has a higher proportion of fibre-oriented transverse to the flow. This results in a CTE mismatch between the two regions. It should be mentioned that the factors affecting the thermal stability are not solely due to orientation effects, but can also be a consequence of the temperature profiles throughout the cavity as the rapidly solidifying shell is expected to shrink first, whilst the core remains relatively warm and reaches the mould temperature at a later stage. Further, as will be seen in later sections, the local deformation of the preform into the rib cavity effectively changes the cross-sectional area that the injected compound is flowing through, thus, for larger deformations it is expected that the measured fibre orientation taken will differ due to the shorter distance between the preform and point of measurement.

Void Content

No voids were observed in the base plate, indicating good consolidation of the base plate. When analysing the ribs at a given location along the flow length, voids were seen to be most common in the core region, where the temperature is hottest for longer and where the fibres experience more movement. This inhomogeneity of the cooling within a given rib cross section gives rise to the thermal stresses. The shell is first to solidify (and shrink), followed by the core region. As the core begins to

shrink, it is hindered by the solidified shell, resulting in a stress distribution, where the shell is in compression and the core is in tension [39]. The size of the core regions varied considerably within each manufactured component, leading to no significant difference in the measured void contents between the rib geometries at the same location. However, further analysis showed a 66 % increase in the size of the core from the start to the end location of Rib 3, as seen in Figure 11a-b, for which the respective void contents were measured to be 0.57 % and 1.17 %. In plastics processing, voids are caused by localised shrinkage of the material at sections with insufficient consolidation and this suggests why the void content increases towards the end of the cavity length, since the pressurisation capability is reduced further away from the gate [23, 40]. Moreover, water desorption in the compound material could be a cause of the voids, although the drying stage prior to overmoulding was taken as a precautionary measure to avoid this. A feasible solution for the elimination of voids would be to increase the pressure profile during the filling and holding stages [41].

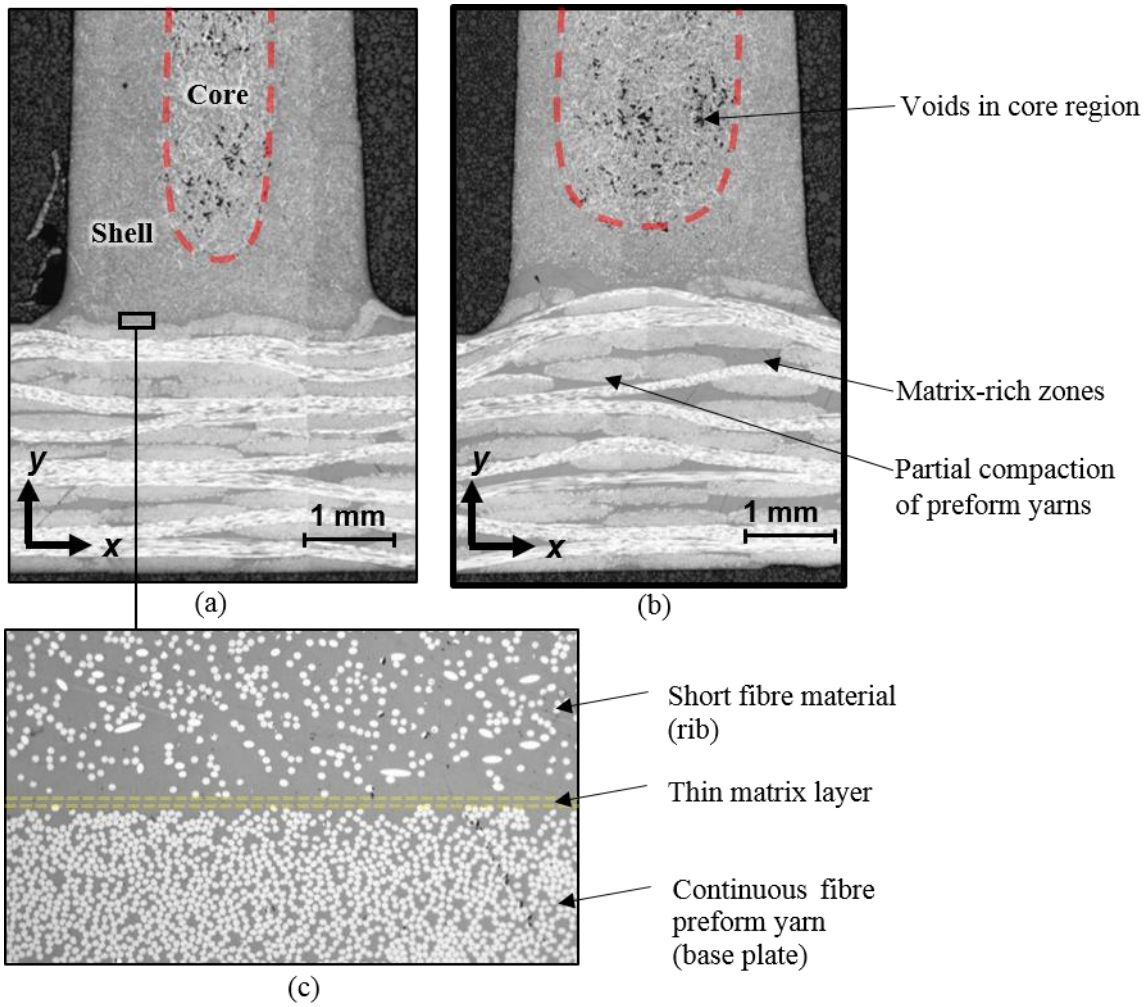

Figure 11: Optical micrographs of the interface of Rib 3 at the start (a) and end (b) locations of the cavity length, with the core size change highlighted by the red-dashed curve. Thin matrix layer bounding the continuous fibre and short fibre materials in the ribbed plate (c).

The presence of a thin matrix layer between the base plate and ribs, as seen in Figure 11c, reveals two key aspects of the consolidation at the overmoulded interface. Firstly, the lack of a visible weld line or voids in this region suggests that intimate contact is achieved between the base plate and the ribs. At temperatures above the melting point, this type of observation can be expected as the matrix from both the preform and compound materials is able to flow and thus coalesce in the absence of a rough surface with asperities. Secondly, the mechanical performance of the joint can be assumed to be solely dependent on the matrix properties, to a first approximation, as there is no evidence of fibre bridging in this thin matrix region between the short fibres and continuous fibres.

Preform Deformation

The consolidation mechanics at the interface between the continuous fibre and short fibre materials are unique to overmoulded components since there is a localised deformation of the preform material, the magnitude of which is seen to increase with the size of the rib foot width. During the forming stage, the preform surface solidifies immediately at the areas in direct contact with the tool halves, whilst the areas exposed to the cavities remain in a both unconstrained and warmer state, due to the relatively lower heat loss. This causes the continuous fibre material to locally protrude into the rib cavities until it is consolidated via the pressurised compound material, forcing it partially back to its original state. The largest deformations at the middle location of the flow path are observed in Rib 4 (0.73 ± 0.10 mm) whilst the smallest are in Rib 3 (0.36 ± 0.03 mm), as can be seen in Figure 12. This implies that there is an increased ability to displace longer unconstrained fibres in the matrix, most likely due to the larger heat footprint observed in the wider ribs.

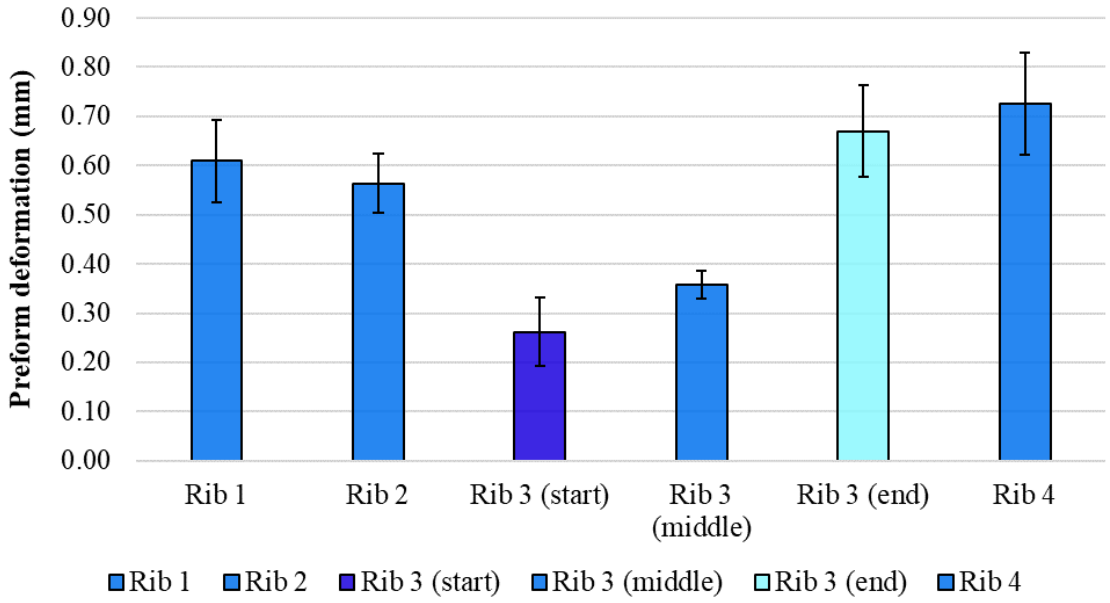

Figure 12: Preform deformations at the overmoulded interface for all specimen cut locations.

The preform deformation is also seen to increase along the length of Rib 3. This effect can be attributed to the variation in the consolidation profiles at the different locations as the compound material takes a finite time to fill and pressurise the cavity. At the start of the rib, the deformation is expected to be the lowest given that the preform material is under compaction for a longer time as well as at a higher temperature due to the rapid interaction with the injected compound material. Towards the end of the rib length, however, the average temperature in the preform will be lower, prior to the arrival of the injected compound, due to the steady heat loss to the colder mould, as predicted by the preliminary MoldFlow results. This results in a more viscous matrix, requiring a higher compaction pressure to force it back to its original state. Further, the heating method used in this manufacturing process may affect the in-plane temperature distribution of the preform due to the rising hot air, causing the bottom of the preform to see a lower heat flux. This is commonly referred to as the "chimney effect" and can affect the consolidation of vertically-heated preforms. Additionally, given that the pressurisation effect of the overmoulded material decreases due to the cavity pressure drop between the start and end of the flow length, the local preform deformation is expected to be higher towards the end. Similar behaviour of the organosheet preform was also observed by Valverde et al. [27] when the holding pressure profile was varied, implying that the state of the interface can be controlled by the pressure of the injected compound material.

Qualitative analysis of the micrographs shows the presence of matrix-rich zones and incomplete compaction of the fibres in overmoulded interfaces with significant levels of preform deformation, as can be evidenced by the clear white areas highlighted in Figure 13. This phenomenon is also initiated during the forming stage as the high compaction pressures (up to 18 MPa) imparted by the tool surface

forces the matrix to flow from the bulk of the base plate towards the cavity, where the material is locally unconstrained. Such effect could be contributing to the local deformation of the preform as the suspended fibres are essentially being pushed upward by the flowing matrix, resulting in partial compaction of the preform and thus fibre path defects locally. Further, the importance of such localised deformations in ribbed plates is highlighted in [42], as the magnitude of the preform deformation was seen to increase with the heating temperature. At sufficiently high temperatures, the effective reduction in rib cross-sectional area can lead to a reduced pressurisation capability for the injected material to fill the cavity, and thus a short shot.

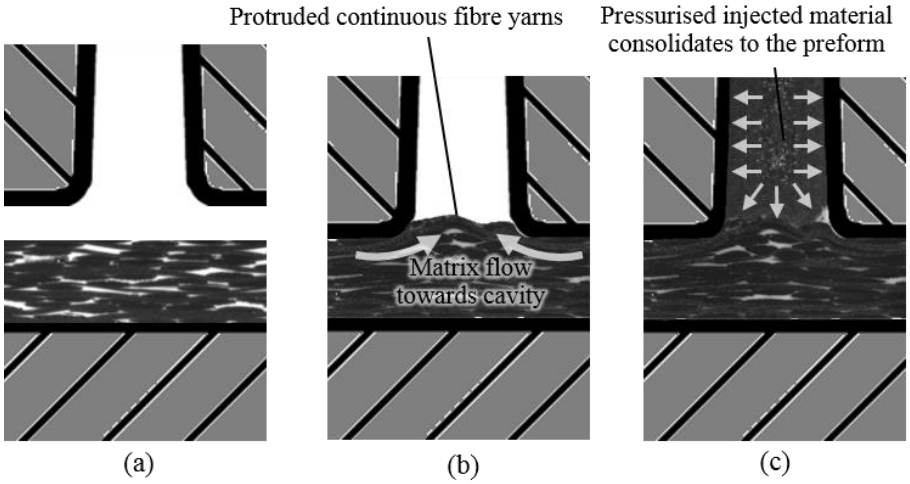

Figure 13: Cross-section micrographs of overmoulded interface evolution throughout the transfer (a), forming (b) and filling + holding (c) stages.

Rib Pull-Off Tests

A variety of failure types are observed for the different samples, as seen in Figure 14. The overmoulded interfaces and base plates of Rib 1 and Rib 4 show little to no sign of damage as the failure occurs at either the rib body (40 % of samples for Rib 1, 60 % of samples for Rib 4) or in the neck region (40 % of samples in Rib 1, 40 % of samples for Rib 4). Only one of the five tested specimens in Rib 1 showed damage in the base plate and interface region. Naturally, fracture in the rib body can be introduced by the clamping jaw pressure, and the change in rib geometry near the neck can result in a stress concentration. Further analysis of the micrographs shows that the vertical position of the neck coincides with the bottom of the core region, where a mismatch in thermal expansion coefficient is expected due to the sharp change in fibre orientation and void content, suggesting that this region is prone to higher levels of residual stress. In contrast, the failure type in Rib 2 and Rib 3 is observed to be more interface-dominated as the crack paths follow the continuous fibre deformation pattern throughout the rib width and also shows minor local delaminations in the base plate. This can be observed by comparing the fracture images to the corresponding cross sections in Figure 14. The dependence of the component failure on the local geometry of the overmoulded joint is particularly noticeable in Rib 2, as the low rib foot depth enables the deformed preform to interact with the mould walls. This causes the preform material to kink upwards and conform to the geometry of the cavity at the edges of the rib, causing the crack path to travel along both the overmoulded interface and the preform material, as can be evidenced by the cracking of the base plate in Figure 14b. It is worth mentioning that 40 % of samples tested in Rib 2 failed at the rib body, whilst the remaining 60 % of samples failed at the interface, where traces of rib material were left on edges of the rib footprint. The fact that failure typically occurs across a non-planar surface in some of the specimens is one of the many reasons as to why accurate characterisation of the interface bonding strength is a challenging task for the geometries considered in this study. The preform weave architecture is also expected to influence the joint performance, given that the size of the rib width in all four designs is less than the woven unit cell size, suggesting a lack of consistency across the overmoulded interfaces of the tested

specimens. This could be addressed by using larger specimen sizes or by using alternative preform materials, to ensure a more regular overmoulded interface for mechanical testing.

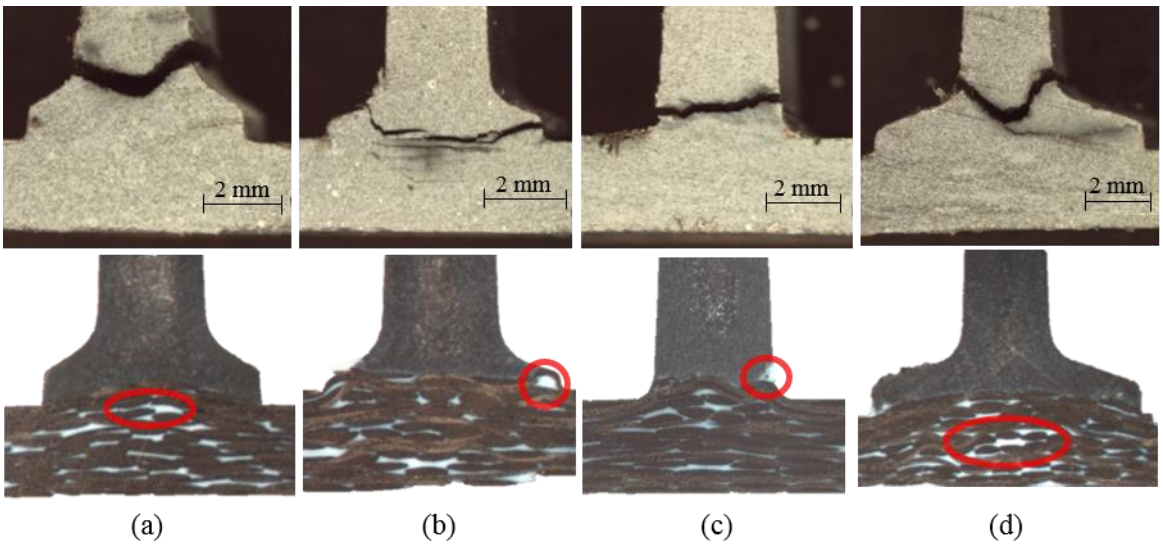

Figure 14: Specimen cross sections and corresponding fracture images for Ribs 1-4 (a-d). Red highlighted areas indicate the presence of matrix-rich zones.

Overall, the mechanical results show that whilst good bonding is achieved at the overmoulded interface, limited information about the interface strength can be extracted, due to the cohesive and mixed failure patterns. The strengths of the different rib-plate joints are shown in Figure. 15. It can be assumed that the strength of the short fibre compound transverse to the flow direction will be similar to the strength of the neat matrix (90 MPa), due to the relatively low fibre orientation in the loaded direction. The measured strengths of Rib 1 and Rib 4 correspond to 46 % and 54 % of the neat PPS matrix strength respectively. Two sets of strengths are presented for Rib 2 according to their failure type, as can be seen in Figure 15, where the specimens that failed in the rib region (these failure types are represented with orange-coloured bars) correspond to 52 % of the neat PPS matrix strength. The high strength variation in the specimens that failed at the interface of Rib 2 could be caused by the interaction of the continuous fibres with the mould cavity as well as the effects of the weave architecture, as previously mentioned. It is also recognised that the error in specimens exhibiting multiple failure types may not present statistical evidence due to the reduced sample size. A steady reduction in the bond strength of Rib 3 is observed when comparing the specimens along the flow length. The lower strengths observed at the end of the flow (25% of neat PPS matrix strength, compared to 32% and 29% at the start and middle locations respectively) suggests that the temperature at the overmoulded interface drops significantly, given that higher temperatures facilitate macromolecular diffusion across the overmoulded interface and promote bond development [43]. From a materials perspective, although the matrix in both the preform and compound are linear polymers, they are supplied by different companies, introducing another potential degree of variability with regards to the bonding. Further, the resulting crystallinity in the manufactured components is known to be dependent on the cooling rate [44, 45]. As overmoulding is a highly non-isothermal process, where the bond between the base plate and ribs is established in a matter of seconds, leading to very high cooling rates, it is likely that the material is in an amorphous state, where strength development via healing may occur below the melting temperature, as has been previously demonstrated in rapid thermoplastic processing technologies such as AFP (Automated Fibre Placement) [46]. Overall, low levels of crystallinity are expected in components manufactured under such conditions, suggesting that a post-processing step may be necessary to fulfil minimum crystallinity requirements. Moreover, it is anticipated that in components with wider ribs (leading to a relatively lower cooling rate compared to ribs with narrower feet), the material has more time to crystallise and hence develop strength. Although crystallisation kinetics are not considered in this

study, it is important to address the effects caused by the relatively high cooling rates in rapid processing techniques in future work.
At the overmoulded interface, the varying levels of preform deformation along the flow length, as previously discussed, implies an effective increase in the local bonding area due to the effective curvature. Although this may lead to higher failure loads, the additional shear components acting along the interface may hinder the structural performance, given that the shear strength of neat PPS is lower than the tensile strength. Nonetheless, the presence of a property gradient along the flow path implies that either the process settings or design of the component must be adjusted to maintain a consistent degree of bonding throughout the final component. This could include increasing the injection speed in order to fill the cavity faster, overcoming the temperature drop in the preform material at locations further away from the gate. However, an increase in injection speed during the filling phase suggests that higher injection pressures will be needed, thus potentially leading to higher running costs.

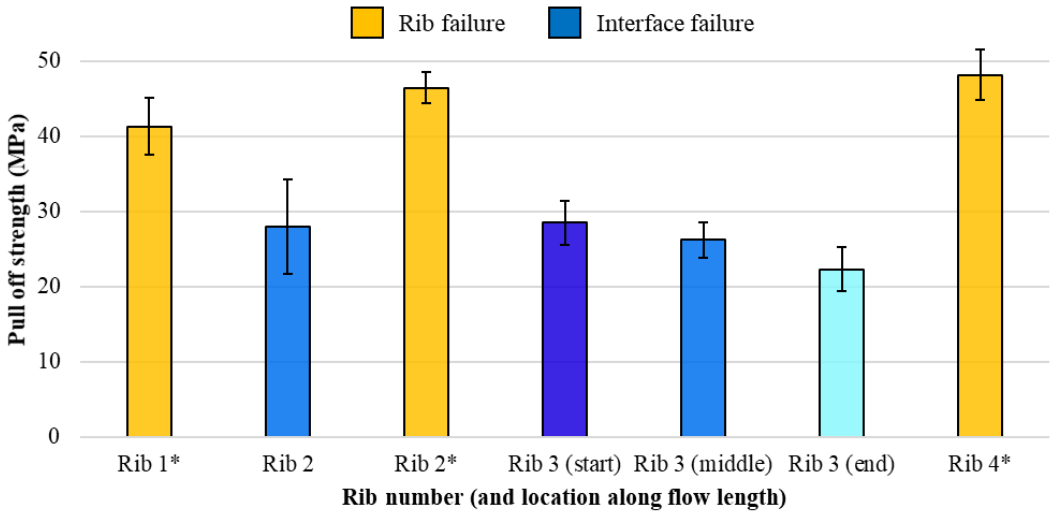

Figure 15: Tensile pull-off force for tested rib specimens. Orange-coloured bars and * indicate that specimens failed in the rib region. Error bars indicate the standard deviation.

Conclusions

In this study, CF/PPS overmoulded ribbed plates were manufactured using a standard injection moulding machine in a 140 s cycle time. The bonding quality between the continuous fibre base plate and the short fibre ribs was assessed via quasi-static rib pull-off tests and analysis of the fracture behaviour. It was demonstrated through specimen micrographs that some of the process-induced features were not only influenced by the choice of rib geometry but also by the location that the specimens were taken from, evidenced by the property variations between the start and end of the injected flow length. In general, very good bonding is achieved between the base plate and ribs, evidenced by the cohesive failure of certain rib designs at higher loads, as opposed to an adhesive-dominated failure at the interface, indicating a weaker joint. This variation in failure type does however imply that the modelling of such components in order to predict mechanical behaviour can become a complex task due to the myriad of process-induced features and geometry-dependent properties developing near the interface and throughout the overmoulded structure. The analysis of such features and properties provides an insight into the consolidation mechanisms taking place during overmoulding and can serve to aid the future design of components. Further work should focus on characterisation of the filling, holding and cooling stages through process simulations in order to capture the full temperature-pressure profiles. This will contribute to the development of the manufacturing knowledge and establishment of thermoplastic composite overmoulding-specific design guidelines for different material systems, mould geometries and processing parameters.

Acknowledgements
The authors would like to acknowledge the EPSRC (EP/P510427/1) and Rolls-Royce Plc for their support of this research through the collaboration of the Composites University Technology Centre (UTC) at the University of Bristol and the Lightweight Structures & Materials UTC at the Technische Universität Dresden.

References
[1] Gabrion, X., Placet, V., Trivaudey, F., & Boubakar, L. About the thermomechanical behaviour of a carbon fibre reinforced high-temperature thermoplastic composite. Composites Part B: Engineering, 2016, 95, 386–394.

[2] Baran, I., Cinar, K., Ersoy, N., Akkerman, R., & Hattel, J. H. A Review on the Mechanical Modeling of Composite Manufacturing Processes. Archives of Computational MethodEngineering, 2017, 24(2), 365–395.

[3] Díaz, J., & Rubio, L. Developments to manufacture structural aeronautical parts in carbon fibre reinforced thermoplastic materials. Journal of Materials Processing Technology, 2003, 143–144(1), 342–346.

[4] Wijskamp S. Shape distortions in composites forming. PhD thesis, University of Twente, the Netherlands, 2005.

[5] Wang, P., Hamila, N., & Boisse, P. Thermoforming simulation of multilayer composites with continuous fibres and thermoplastic matrix. Composites Part B: Engineering, 2013, 52, 127–136.

[6] Dallner, C., Schnorr, J., Wollny, A., Radtke, A., Henningsen, M., Vandermeulen, G., … Sandler, J. K. W. Materials for the future of lightweight construction. Kunststoffe International, 2012, 102(3), 30–35.

[7] Bouwman, M. B., Donderwinkel, T., Krämer, E., Wijskamp, S., and Costa, F. Overmolding - An integrated design approach for dimensional accuracy and strength of structural parts. In: CAMX 2016 - Composites and Advanced Materials Expo, 2016.

[8] Hufenbach W., Langkamp A., Adam F., Krahl M., Hornig A., Zscheyge M., Modler, N. An integral design and manufacturing concept for crash resistant textile and long-fibre reinforced polypropylene structural components. In: 11th International Conference on the Mechanical Behaviour of Materials, 2011, p. 2086-2091.

[9] Liebsch, A., Kupfer, R., Krahl, M., Haider, D., Koshukow, W., Gude, M. Adhesion Studies of Thermoplastic Fibre-Plastic Composite Hybrid Composites Part 1: Thermoplastic-Thermoplastic-Composites (In Press), In: 3rd International Conference on Hybrid Materials and Structures, 2018.

[10] Al-Sheyyab A.: Light-Weight Hybrid Structures – Process Integration and Optimized Performance. Dissertation, Erlangen, 2008.

[11] Jaroschek, C. The Construction Material of The Future. Kunststoffe International, 2010, (9), 16–20.

[12] LANXESS Deutschland GmbH, ZF Friedrichshafen AG, Case study, Brake pedal in polyamide composite sheet hybrid technology, 2014.

[13] Barfuss, D., Garthaus, C., Kupfer, R., Schemm, F., Injection forming of gears on high performance CF-PAEK drive shafts, 4th International Conference & Exhibition on Thermoplastic Composites, Bremen, 2018.

[14] Kunststoffe International, Cost Efficient Production of Complex Aircraft Parts, Hanser Publishers, 2019.

[15] Yang, F., & Pitchumani, R. Healing of thermoplastic polymers at an interface under nonisothermal conditions. Macromolecules, 2003, 35(8), 3213–3224.

[16] L. Tong and G. P. Stevens, Analysis and Design of Structural Bonded Joints. Kluwer Academic Publishers, Dordrecht, The Netherlands, 1999.

[17] Schell, J. S. U., Guilleminot, J., Binetruy, C., & Krawczak, P. Computational and experimental analysis of fusion bonding in thermoplastic composites: Influence of process parameters. *Journal of Materials Processing Technology*, *209*(11), 5211–5219, 2009.

[18] Plummer, C. J. G., Bourban, P. E., Zanetto, J. E., Smith, G. D., & Månson, J. A. E. Nonisothermal fusion bonding in semicrystalline thermoplastics. *Journal of Applied Polymer Science*, 2002, *87*(8), 1267–1276.

[19] Jud, K., Kausch, H. H., & Williams, J. G. Fracture mechanics studies of crack healing and welding of polymers, 1981, *16*, 204–210.

[20] Giusti, R., & Lucchetta, G. Modeling the adhesion bonding mechanism in overmolding hybrid structural parts for lightweight applications. Key Engineering Materials, 2014, 611–612, 915–921.

[21] Bernasconi, A., Cosmi, F., & Dreossi, D. Local anisotropy analysis of injection moulded fibre reinforced polymer composites. Composites Science and Technology, 2008, 68(12), 2574–2581.

[22] Vincent, M., Giroud, T., Clarke, A., & Eberhardt, C. Description and modeling of fiber orientation in injection molding of fiber reinforced thermoplastics. Polymer, 2005, 46(17), 6719–6725.

[23] Vaxman, A., Narkis, M., Siegmann, A., & Kenig, S. Void formation in short-fiber thermoplastic composites. Polymer Composites, 1989, 10(6), 449–453.

[24] Bernasconi, A., Cosmi, F., & Hine, P. J. Analysis of fibre orientation distribution in short fibre reinforced polymers: A comparison between optical and tomographic methods. Composites Science and Technology, 2012, 72(16), 2002–2008.

[25] Joppich, T., Menrath, A., & Henning, F. Advanced Molds and Methods for the Fundamental Analysis of Process Induced Interface Bonding Properties of Hybrid, Thermoplastic Composites. Procedia CIRP, 2017, 66, 137–142.

[26] Stegelmann M., Krahl M., Garthaus C., Hufenbach., W., Integration of textile reinforcements in the injection-moulding process for manufacturing and joining thermoplastic support-frames. In: 20th international conference on composite materials (ICCM), 2015.

[27] Valverde, M. A., Kupfer, R., Kawashita, L. F., Gude, M., & Hallett, S. R. Effect of Processing Parameters on Quality and Strength in Thermoplastic Composite Injection Overmoulded Components, ECCM18 – 18th European Conference on Composite Materials, 2018.

[28] R. Gaitzsch, M. Koerdt and A.S. Herrmann, Suitable Coupon Design for Assessment of Interface Strength in Overmoulded Structures made from Fibre Reinforced High-performance Thermoplastics, Proceedings of the 4th International Conference & Exhibition on Thermoplastic Composites, Bremen, Germany, Paper E4, 2018, pp. 108-111, 2018.

[29] Valverde, M. A., Kupfer, R., Kawashita, L. F., Gude, M., & Hallett, S. R. Influence of Geometry on Component Quality in Overmoulded Thermoplastic Composite Parts, FPCM14 – 14th International Conference on Flow Processes in Composite Materials, 2018.

[30] Ma, C. M., & Yur, S. -W. Environmental effects on the water absorption and mechanical properties of carbon fiber reinforced PPS and PEEK composites. Part II. Polymer Engineering & Science, 1991, 31(1), 34–39.

[31] Grouve W. J. B., Weld strength of laser-assisted tape-placement thermoplastics composites, University of Twente, 2012.

[32] Yousefpour, A., Hojjati, M., & Immarigeon, J. P. Fusion bonding/welding of thermoplastic composites. Journal of Thermoplastic Composite Materials, 2004, 17(4), 303–341.

[33] TenCate Cetex® TC1100 PPS resin system, Product datasheet, TenCate Advanced Composites, 2016 .

[34] Nian, S. C., Wu, C. Y., & Huang, M. S. Warpage control of thin-walled injection molding using local mold temperatures. International Communications in Heat and Mass Transfer, 2015, 61(1), 102–110.

[35] Advani, S. G. The Use of tensors to describe and predict fiber orientation in short fiber composites. Journal of Rheology, 1987, 31(8), 751.

[36] Santulli, C., Gil, R. G., Long, A. C., & Clifford, M. J. Void content measurements in commingled E-Glass/ polypropylene composites using image analysis from optical micrographs. Science and Engineering of Composite Materials, 2002, 10(2), 77–90.

[37] Bay, R. S., & Tucker, C. L. Fiber orientation in simple injection moldings. Part I: Theory and numerical methods. Polymer Composites, 1992, 13(4), 317–331.

[38] Akay, M., & Barkley, D. Fibre orientation and mechanical behaviour in reinforced thermoplastic injection mouldings. Journal of Materials Science, 1991, 26(10), 2731–2742.

[39] Depolo, W. S. Dimensional Stability and Properties of Thermoplastics Reinforced with Particulate and Fiber Fillers By Dimensional Stability and Properties of Thermoplastics Reinforced with Particulate and Fiber Fillers. *Doctor of Philosophy*, 2005.

[40] Leblanc, D., Landry, B., Levy, A., Hubert, P., Roy, S., Yousefpour, & Quilan, E. A. Study of Processing Conditions on the Forming of Ribbed Features, Journal of the American Helicopter Society, 2015, 60(1), 1–9.

[41] Vipond, R., & Daniels, C. J. Non-destructive examination of short carbon fibre-reinforced injection moulded thermoplastics. Composites, 1985, 16(1), 14–18.

[42] Valverde, M. A., Kupfer, R., Kawashita, L. F., Gude, M., & Hallett, S. R. An experimental study on the preform evolution during thermoplastic composite overmoulding, ICCM22 – 22nd International Conference on Composite Materials, 2019.

[43] Awaja, F. Autohesion of polymers. Polymer (United Kingdom), 2016, 97, 387–407.

[44] Spruiell, J. E., Janke, C. J., Case, S. W., & Reifnider, K. L. A review of the measurement and development of crystallinity and its relation to properties in neat PPS and its fiber reinforced composites. In *Time depend and nonlinear effects in polymers and composites*, 2004.

[45] Batista, N. L., Olivier, P., Bernhart, G., Rezende, M. C., & Botelho, E. C. Correlation between degree of crystallinity, morphology and mechanical properties of PPS/carbon fiber laminates. *Materials Research*, 2016, *19*(1), 195–201.

[46] Stokes-Griffin, C. M., & Compston, P. Investigation of sub-melt temperature bonding of carbon-fibre/PEEK in an automated laser tape placement process. *Composites Part A: Applied Science and Manufacturing*, 2016, *84*, 17–25.